K-fiber bundles in the mitotic spindle are mechanically reinforced by Kif15

Marcus A. Begley[a], April L. Solon[b], Elizabeth Mae Davis[a], Michael Grant Sherrill[a], Ryoma Ohi[b], and Mary Williard Elting[a,c,*]

[a]Department of Physics, North Carolina State University, Raleigh, NC 27607; [b]Department of Cell & Developmental Biology, University of Michigan, Ann Arbor, MI 48109; [c]Quantitative and Computational Developmental Biology Cluster, North Carolina State University, Raleigh, NC 27695

ABSTRACT **The mitotic spindle, a self-constructed microtubule-based machine, segregates chromosomes during cell division. In mammalian cells, microtubule bundles called kinetochore fibers (k-fibers) connect chromosomes to the spindle poles. Chromosome segregation thus depends on the mechanical integrity of k-fibers. Here we investigate the physical and molecular basis of k-fiber bundle cohesion. We detach k-fibers from poles by laser ablation-based cutting, thus revealing the contribution of pole-localized forces to k-fiber cohesion. We then measure the physical response of the remaining kinetochore-bound segments of the k-fibers. We observe that microtubules within ablated k-fibers often splay apart from their minus-ends. Furthermore, we find that minus-end clustering forces induced by ablation seem at least partially responsible for k-fiber splaying. We also investigate the role of the k-fiber-binding kinesin-12 Kif15. We find that pharmacological inhibition of Kif15-microtubule binding reduces the mechanical integrity of k-fibers. In contrast, inhibition of its motor activity but not its microtubule binding ability, i.e., locking Kif15 into a rigor state, does not greatly affect splaying. Altogether, the data suggest that forces holding k-fibers together are of similar magnitude to other spindle forces, and that Kif15, acting as a microtubule cross-linker, helps fortify and repair k-fibers. This feature of Kif15 may help support robust k-fiber function and prevent chromosome segregation errors.**

Monitoring Editor
Claire Walczak
Indiana University

Received: Jun 30, 2020
Revised: Sep 27, 2021
Accepted: Oct 7, 2021

INTRODUCTION

The mitotic spindle is a microtubule-based machine responsible for accurate chromosome segregation during cell division. In order for spindles to perform their essential function, they must be both robust and adaptable in a highly dynamic cellular environment. Kinetochore fibers (k-fibers), microtubule bundles that link centrosomes to chromosomes, must therefore also be both robust and dynamic (Rieder, 1981; Hays *et al.*, 1982; McDonald *et al.*, 1992). Indeed, while single spindle microtubules turn over in ~15 s, k-fibers are more stable and turn over on the order of minutes (Saxton *et al.*, 1984; Mitchison, 1989; McDonald *et al.*, 1992; Zhai *et al.*, 1995). Yet, k-fibers must not be too stable, or spindles become compromised in their ability to correct attachment errors, which can result in chromosome missegregation (Lampson *et al.*, 2004). The lifetime of microtubules is therefore adjusted to promote proper spindle function through the action of many proteins that control microtubule dynamics (Walczak, 2000; Drummond, 2011; Brouhard and Rice, 2018). Regulation of microtubule lifetime is not the only way that spindles respond to competing demands: a growing body of evidence shows that force generation in the spindle balances robustness and dynamics in myriad ways (Pereira and Maiato, 2012; Elting *et al.*, 2014, 2017; Kajtez *et al.*, 2016; Long *et al.*, 2020; Suresh *et al.*, 2020). Yet, how k-fibers tune their mechanical integrity to maintain spindle structure and support accurate chromosome segregation remains unclear.

K-fibers are a largely parallel array of microtubules that span the distance from the pole to the kinetochore (Rieder, 1981; McDonald *et al.*, 1992). While ~half of these microtubules are contiguous from kinetochore to pole, at least in some cell types (McDonald *et al.*, 1992), a subset of microtubules closely associated with the k-fiber

This article was published online ahead of print in MBoC in Press (http://www.molbiolcell.org/cgi/doi/10.1091/mbc.E20-06-0426) on October 20, 2021.

The authors declare no competing financial interests.

*Address correspondence to: Mary Williard Elting (mary.elting@ncsu.edu).

Abbreviations used: k-fiber, kinetochore fiber; NuMA, Nuclear Mitotic Apparatus protein; STLC, S-trityl-L-cysteine.

are not end-on attached at the kinetochore. Here we use the term k-fiber to include both kinetochore-microtubules and the non-kinetochore-microtubules that closely associate with them. Kinetochores hold together kinetochore-microtubules at their plus-ends, while pole clustering forces, most notably provided by Nuclear Mitotic Apparatus protein (NuMA) and dynein, hold k-fibers together at their minus-ends (Merdes *et al.*, 1996; Gaglio *et al.*, 1997; Dionne *et al.*, 1999). Global disruption of either kinetochores or poles, e.g., by RNA interference, alters spindle architecture as a whole, making it difficult to determine whether end-based clustering is sufficient for stabilizing k-fibers. Furthermore, evidence also suggests that lateral cross-links along the length of the k-fiber help to reinforce the k-fiber and alter its mechanical properties. K-fiber bundles appear to be much straighter and stiffer than individual microtubules (Goshima *et al.*, 2005) and rupture collectively when subjected to sufficient force (Long *et al.*, 2020).

K-fiber reinforcement could come from connections between kinetochore-microtubules themselves or from associations with non-kinetochore-microtubules, which may play an integral role in strengthening the bundle. Non-kinetochore-microtubules that associate with k-fibers include both bridging microtubules, which form an antiparallel bundle spanning the centromere that integrates with each sister k-fiber near the kinetochore (Kajtez *et al.*, 2016), and other spindle microtubules, which often interdigitate at an angle (McDonald *et al.*, 1992). Electron microscopy, microneedle, and laser ablation experiments all indicate that non-kinetochore-microtubules form mechanical connections with kinetochore-microtubules within the k-fiber (Nicklas *et al.*, 1982; Hays and Salmon, 1990; McDonald *et al.*, 1992; Kajtez *et al.*, 2016; Elting *et al.*, 2017; Suresh *et al.*, 2020). While it is now clear that these non-kinetochore-microtubules contribute to local force dissipation across the spindle, they may also play a role in mechanical stabilization of the k-fiber itself.

Despite this evidence that they do so, it is not yet clear *how* interactions along the lengths of k-fiber microtubules, such as those through microtubule cross-linkers, contribute to the dynamic behavior and temporal longevity of the k-fiber as a whole (Elting *et al.*, 2018). A handful of microtubule-associated proteins, such as the kinesin-12 Kif15 (Sturgill *et al.*, 2014) and its regulator TPX2 (Bird and Hyman, 2008; Sturgill *et al.*, 2014; Mann *et al.*, 2017), the clathrin/chTOG/TACC3 complex (Royle *et al.*, 2005; Booth *et al.*, 2011; Cheeseman *et al.*, 2013; Nixon *et al.*, 2015), HURP (Silljé *et al.*, 2006; Tsuchiya *et al.*, 2018), and kinesin Kif18A (Mayr *et al.*, 2007; Ye *et al.*, 2011), have been shown to localize preferentially to k-fibers and/or to stabilize them, thereby promoting efficient and reliable mitotic progression. However, their precise contributions to k-fiber mechanics and force production remain an open question.

The kinesin-12 Kif15 is well positioned to shape k-fiber mechanics through both passive cross-linking and active force production. Like the kinesin-5 Eg5, a plus-end-directed motor responsible for separating poles in prometaphase to establish spindle bipolarity (Kapoor *et al.*, 2000), Kif15 is capable of cross-linking microtubule pairs and sliding antiparallel microtubules apart (Kapitein *et al.*, 2005; Drechsler *et al.*, 2014; Reinemann *et al.*, 2017). Through this mechanism, Kif15 can antagonize inward forces generated by minus-end-directed motors, thereby enforcing spindle bipolarity and separating centrosomes in cells adapted to grow in the presence of Eg5 inhibitors (Raaijmakers *et al.*, 2012; Sturgill and Ohi, 2013). This redundancy between Kif15 and Eg5 is of interest as a potential factor in the disappointing ineffectiveness thus far of Eg5 inhibitors as cancer therapeutics (Tanenbaum *et al.*, 2009; Rath and Kozielski, 2012; Milic *et al.*, 2018; Dumas *et al.*, 2019). Kif15 may also have uncharacterized roles in other aspects of kinetochore-microtubule attachment, suggested by data showing that overexpression of Kif15 results in lagging chromosomes (Malaby *et al.*, 2019). In this light, it is notable that Kif15 is up-regulated in a number of cancers (Ma *et al.*, 2014; Wang *et al.*, 2017; Qiao *et al.*, 2018; Yu *et al.*, 2019; Zhao *et al.*, 2019; Sun *et al.*, 2020; Terribas *et al.*, 2020). Under normal circumstances, however, Kif15 localizes predominantly to k-fiber microtubules. Its function on k-fibers is largely unexplored, although it is presumably from this location that the motor slides antiparallel microtubules apart.

Overall, the localization and known functions of Kif15 indicate that it might contribute to the mechanical properties of k-fibers. In addition, some evidence suggests that Kif15 coordinates the movement of neighbor sister kinetochores within the spindle (Vladimirou *et al.*, 2013). While it remains unclear whether Kif15 oligomerizes as a dimer or tetramer in vivo (Drechsler *et al.*, 2014; Mann *et al.*, 2017; Reinemann *et al.*, 2017), its second microtubule binding site, in addition to its motor domain, gives it inherent microtubule bundling ability even in a dimeric state (Sturgill *et al.*, 2014). Yet, Kif15 requires its binding partner, TPX2, for recruitment to the spindle (Tanenbaum *et al.*, 2009). Furthermore, in vitro data indicate that TPX2 increases Kif15 microtubule binding while decreasing motor activity (Drechsler *et al.*, 2014; Mann *et al.*, 2017; McHugh *et al.*, 2018), raising the question of how important motor activity is for its function on k-fibers.

To understand the dynamics and structural maintenance of the k-fiber, we mechanically disrupted k-fibers in the mitotic spindles of mammalian Ptk2 kidney epithelial cells. First, we used laser ablation to detach k-fibers from poles, disrupting forces that may hold them together at their minus-ends. We found that the microtubules of these detached k-fibers often splay apart, and that this splaying results from minus-end clustering forces that can outcompete bundling forces. Next, to probe the role of Kif15 in k-fiber integrity, we examined k-fiber splaying in cells treated with two Kif15 inhibitors that operate through two different mechanisms. Ablation experiments in cells treated with GW108X, which inhibits Kif15's microtubule cross-linking activity, revealed a heightened sensitivity to minus-end-directed forces. In contrast, we did not observe this effect in cells treated with Kif15-IN-1, which locks Kif15 into a tight microtubule-binding state and thus promotes microtubule cross-linking. The data presented here suggest that, independently of its motor activity, Kif15 mechanically reinforces k-fiber structure by binding to and cross-linking k-fiber microtubules. The bundling forces provided at least in part by Kif15 are of a strength that allows them to compete with minus-end clustering forces, suggesting they play a mechanical role in preserving the integrity of k-fibers, thus supporting accurate chromosome alignment and segregation.

RESULTS AND DISCUSSION

K-fibers are dynamically held together along their lengths by connections that can be disrupted and reformed

Using metaphase Ptk2 cells expressing GFP-α-tubulin, we performed laser ablations to remove forces holding k-fibers together at minus-ends and determine the degree to which k-fibers remain cohesive along their lengths (Figure 1A). The mechanical response to ablation commonly consisted of two readily observed behaviors, "poleward transport" and a behavior we term "splaying." Poleward transport, a well-documented response to detached minus-ends (Elting *et al.*, 2014; Sikirzhytski *et al.*, 2014), followed nearly all ablations (Figure 1, B and C; Supplemental Figure S1A; Supplemental Videos S1 and S2). During splaying, microtubules associated with the k-fiber stub dissociate along their lengths, losing the tightly cohesive appearance typically associated with k-fibers (Figure 1C;

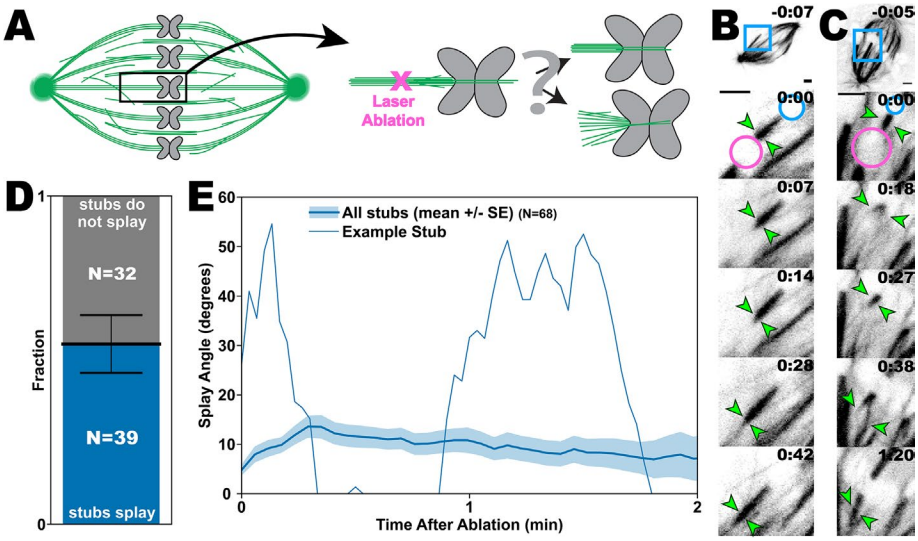

FIGURE 1: K-fiber microtubule bundles often splay apart following detachment from the pole by laser ablation. (A) Schematic of k-fiber ablation experiment. Following ablation (magenta "X"), k-fiber stubs demonstrate either "no splaying" (top) or splaying (bottom). (B, C) Typical examples of k-fiber stubs in Ptk2 cells, expressing GFP-α-tubulin, that do not splay (B) and that do splay (C). The ablation spot (magenta circle), k-fiber stub (green arrows), and chromosomes (blue circle) are labeled in the first postablation frame for both k-fiber stubs. All scale bars are 2 μm and time stamps are in min:sec. (D) Roughly half of ablated k-fiber stubs splay at some point during spindle repair. Error bar indicates the square root of the number of splayed events as an estimate on the variation in this number assuming Poisson statistics. (E) Example trace (narrow blue line) showing the angle over time of a single ablated k-fiber stub and the average (bold blue line) angle of all stubs. Although the average splay angle gradually increases to about 13° before gradually decreasing, splaying varies widely among individual k-fiber stubs, with many splaying and zipping up multiple times and at different points during repair. The shaded region represents average ± SE on the mean.

Supplemental Video S1). When this occurs, microtubule plus ends remain attached at the kinetochore, while the presumed minus ends come apart. This k-fiber stub splaying occurs following ~half of all ablations (Figure 1D). While in general the observable k-fiber stub terminates at the kinetochore, in some cases, we observe that some microtubules associated with the k-fiber stub continue past the kinetochore; we presume these microtubules have mechanical associations with both the k-fiber and the bridging fiber. In all cases, we cannot determine which of the splayed microtubules directly connect to kinetochore at their plus-ends and which may continue past the kinetochore (as part of the bridging fiber). However, we expect that most microtubules that persist after ablation are oriented with their minus-end exposed, since ablated plus-ends are typically unstable and lead to microtubule depolymerization (Spurck *et al.*, 1990; Maiato *et al.*, 2004; Brugués *et al.*, 2012; Sheykhani *et al.*, 2013).

When stubs splay, they typically separate into only two microtubule bundles (Figure 1C). The average amount of splaying increases for the first ~20 s after ablation and remains roughly level after that (Figure 1E). However, the timing, duration, and repetition of these splaying events is highly variable among individual k-fiber stubs. For instance, after a k-fiber stub splays, the splayed microtubule bundles will usually "zip up," reforming into a single tightly bound k-fiber, a process that appears to occur simultaneously all along the k-fiber stub's length. While this connection visually appears complete, it is often not final, as many k-fiber stubs undergo multiple splay–zip cycles during spindle repair (Figure 1C, panels at 0:18 and 0:38, and Figure 1E). Therefore, even though the collective average splay angle provides insight into the overall magnitude and timescale of k-fiber stub splaying, aggregate metrics obscure the significant temporal variability of behavior among individual k-fiber stubs (Figure 1E). This variation suggests an active competition between forces that bind neighboring k-fiber microtubules along their lengths and forces that pull on microtubule minus-ends.

Minus-end clustering forces can overpower bundling forces to pry apart ablated k-fibers

Nearly all k-fiber stubs that splayed did so after the activation of machinery that pulls new minus-ends poleward (Figure 2A). Furthermore, the ability to maintain lateral intermicrotubule connections within k-fiber stubs is somewhat velocity dependent, as k-fiber stubs that were splaying at any given moment experienced a greater poleward velocity than those that were not currently splaying (Figure 2B). These data suggest that forces that cluster minus-ends can also promote splaying, with increasing probability of splaying for k-fiber stubs experiencing stronger minus-end clustering forces.

NuMA has been shown to be required for rapid and robust poleward transport of loose spindle microtubule minus ends, ensuring the maintenance of spindle poles (Elting *et al.*, 2014; Sikirzhytski *et al.*, 2014). NuMA is recruited to these minus ends when they appear and in turn recruits cytoplasmic dynein and dynactin (Hueschen *et al.*, 2017), coalescing NuMA/dynein/dynactin complexes to the ablated k-fiber stub minus-end. Dynein motors, which are minus-end-directed, bind to another spindle microtubule and exert minus-end-directed force on the NuMA-bound microtubule, thereby transporting the k-fiber stub poleward as their cargo (Elting *et al.*, 2014; Sikirzhytski *et al.*, 2014). Because of the apparent dependence of k-fiber stub splaying on poleward transport, we next investigated the potential role of NuMA in splaying. To do so, we performed ablation experiments in mitotic cells depleted of NuMA (Figure 2C, Supplemental Figure S1B). As in previous work (Elting *et al.*, 2017), we chose spindles that retained bipolarity, indicative of only partial NuMA depletion, to increase the chance that any effects that we observed would be the direct result of NuMA perturbation rather than indirect effects from altering overall spindle architecture. As expected due to NuMA's known involvement in poleward transport (Elting *et al.*, 2014; Hueschen *et al.*, 2017), poleward transport begins later and is more gradual for ablated k-fiber stubs in NuMA siRNA cells compared with those in control cells (Supplemental Figure S1C).

Based on NuMA's established role as a mitotic spindle cross-linker, as well as its role anchoring k-fibers in the spindle body (Gaglio *et al.*, 1996; Elting *et al.*, 2017), we initially hypothesized that NuMA might itself mechanically bridge neighbor microtubules in the k-fiber. Strikingly, NuMA depletion resulted in more robust k-fiber bundling, as splaying of ablated k-fiber stubs is much more gradual initially and remains reduced throughout spindle repair (Figure 2, D–F). Thus, it seems that the NuMA/dynein/dynactin complex, functioning as a minus-end-directed force generator, primarily

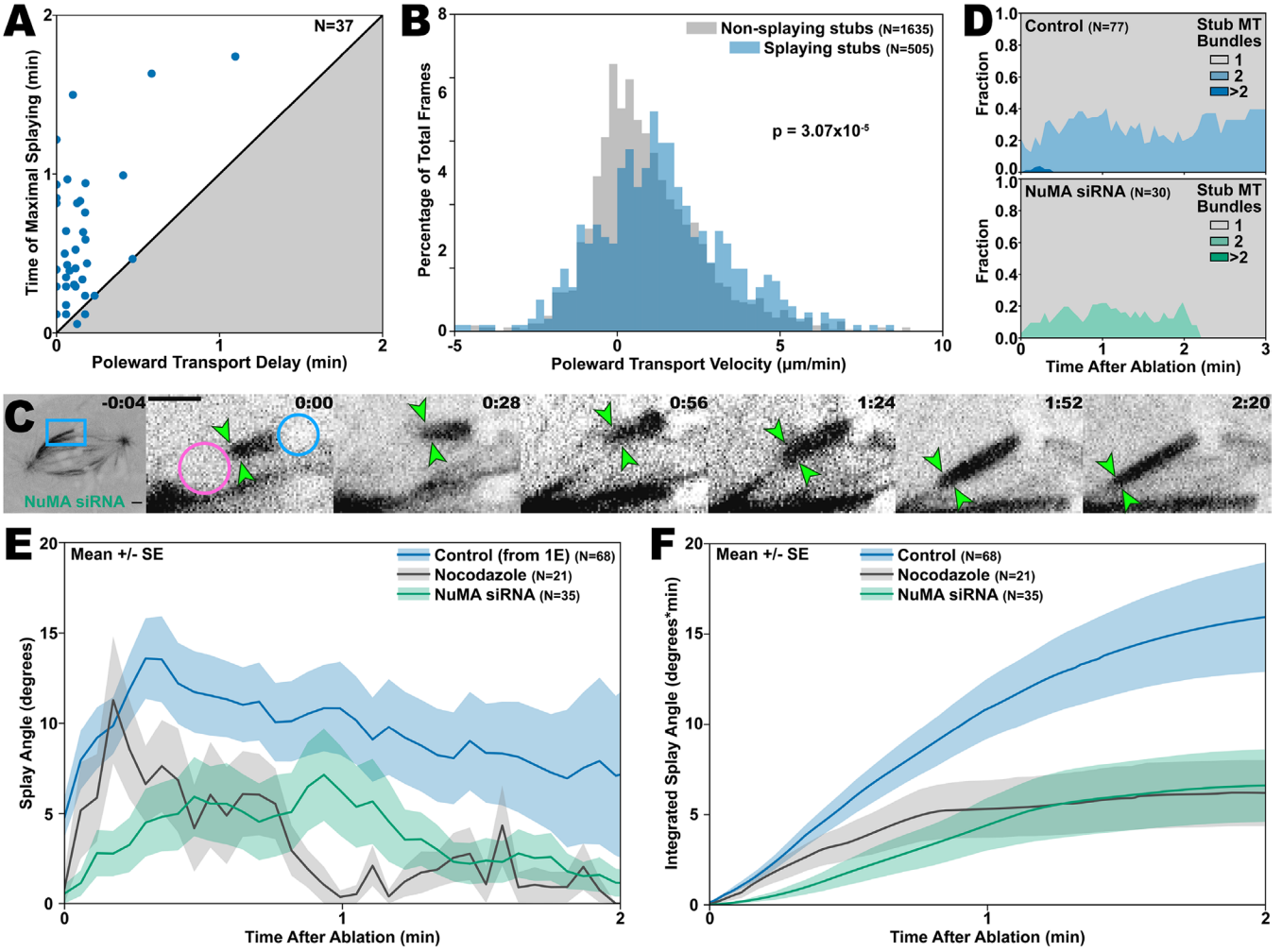

FIGURE 2: Minus-end clustering forces recruited in response to ablation increase the degree to which k-fiber bundles splay apart. (A) The moment of maximal splaying typically follows the onset of poleward transport for untreated k-fiber stubs. Points represent individual k-fiber stubs. Line shows x = y; the white region indicates that maximal splaying follows poleward transport, while the gray region indicates maximal splaying that precedes poleward transport. (B) K-fiber stubs undergoing rapid poleward transport are more likely to splay. Here the *x*-axis is the instantaneous poleward transport velocity and the *y*-axis is the percentage of time points in each histogram bin. (C) Example of an ablated k-fiber stub in a spindle of a Ptk2 cell expressing GFP-α-tubulin treated with NuMA siRNA. Following ablation, the k-fiber stub is transported poleward without splaying. The ablation spot (magenta circle), k-fiber stub (green arrows), and chromosomes (blue circle) are labeled in the first postablation frame. All scale bars are 2 μm and time stamps are in min:sec. (D) K-fiber stubs in spindles treated with NuMA siRNA (bottom, green) splay later than k-fiber stubs from control cells (top, blue) and do not stay splayed for as long. The *y*-axis represents the fraction of k-fiber stubs at each time point, consisting of one, two, or more than two visibly distinguishable microtubule bundles. (E) Splaying is reduced in nocodazole (gray) or NuMA siRNA (green) treated cells compared with untreated cells (blue). Shaded regions represent average ± SE on the mean. Note: these data for control k-fiber stubs were also shown in Figure 1E. (F) Total cumulative splaying, measured as the integration of data shown in E, is lower in cells treated with nocodazole or NuMA siRNA. Shaded regions represent average ± SE on the mean.

works to pry ablated k-fiber stubs apart rather than hold them together. We hypothesize that this occurs due to dynein motors being recruited to multiple track microtubules within the stub that are not precisely parallel. If this were indeed the case, we should observe a reduction in splaying of stubs with fewer microtubule tracks available for effective poleward transport. To test this hypothesis, we ablated k-fibers in cells treated with nocodazole, a small molecule that favors microtubule depolymerization and at low doses can preferentially depolymerize unbundled microtubules (Cassimeris and Salmon, 1991). As expected, lowering the density of available spindle microtubule tracks resulted in reduced splaying despite normal stub poleward transport, which we attribute to lower microtubule density, making it more likely for repair to happen along a single microtubule track (Figure 2, E and F; Supplemental Figure S1D). These data reinforce the hypothesis that minus-end-directed forces involved in poleward transport frequently contribute to longitudinal dissociation of microtubules within the k-fiber from each other.

Kif15 binds and cross-links k-fiber microtubules to promote k-fiber cohesion

We next used pharmacological inhibition to test a potential role for the plus-end-directed cross-linking motors Eg5 and Kif15 in k-fiber

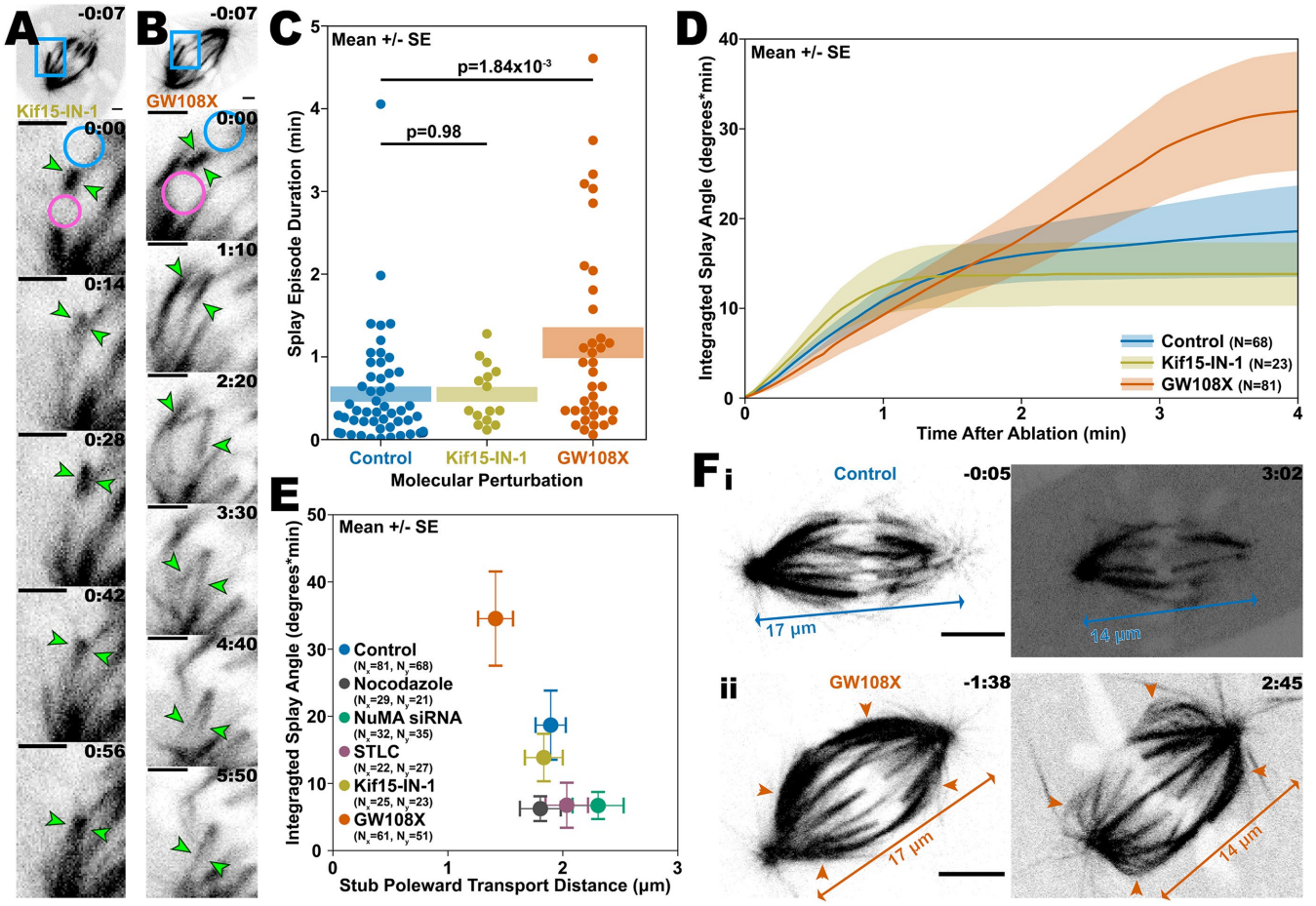

FIGURE 3: Cross-linking from Kif15 mediates the mechanical integrity of the k-fiber. (A, B) Typical examples of behavior of ablated k-fibers in spindles of Ptk2 cells treated with Kif15 inhibitor KIF15-IN-1 (A) and GW108X (B). The ablation spot (magenta circle), k-fiber stub (green arrows), and chromosomes (blue circle) are labeled in the first postablation frame of each panel. All scale bars are 2 μm and time stamps are in min:sec. (C) Kif15 inhibition by GW108X prolongs splaying. The *y*-axis is the length of time between when a k-fiber stub begins splaying and when the k-fiber stub is zipped up. Shaded regions represent average ± SE on the mean and numbers at the top of the plot represent *p* values. (D) Total cumulative splaying, measured by integrating the k-fiber stub splay angle over time, is greater for k-fiber stubs in cells treated with GW108X (which inhibits cross-linking) but is about the same for k-fiber stubs in cells treated with KIF15-IN-1 (which solely inhibits motor activity) when compared with control k-fiber stubs. Shaded regions represent average ± SE on the mean. (E) Although treatment with GW108X reduces the poleward transport of ablated k-fiber stubs, relative to k-fiber stubs in untreated cells, these stubs still exhibit greater total splaying. In contrast, treatment with KIF15-IN-1 does not meaningfully alter the total amount of splaying. Whiskers represent average ± SE on the mean. (F) Unablated k-fibers usually remain tightly bound throughout metaphase in control spindles (i), while outer k-fibers (arrows) in spindles from GW108X-treated cells (ii) sometimes buckle and splay, while still attached at both the pole and kinetochore (example splaying k-fibers, orange arrows). Due to photobleaching, brightness and contrast of later time points are adjusted compared with earlier ones. Scale bars are 5 μm, time stamps are in min:sec, and spindle length at each time point is marked.

cohesion. Based on the fact that poleward transport has been shown to be slightly faster but largely unchanged with Eg5 inhibition (Elting *et al.*, 2014), we expected that the splaying behaviors of ablated k-fiber stubs would remain unchanged (or potentially even increase) with the inhibition of Eg5. For Eg5 inhibition, we selected spindles that had already assembled as Eg5 is not required for bipolarity maintenance in PtK cells (Cameron *et al.*, 2006). Indeed, both the poleward transport and the splaying of ablated k-fiber stubs in S-trityl-L-cysteine (STLC)-treated spindles are generally similar to that of k-fiber stubs in untreated spindles (Supplemental Figure S1, A and C). On the other hand, pharmacological inhibition of Kif15 revealed a more specific role for this motor in k-fiber mechanics (Figure 3). For these experiments, we used two Kif15 inhibitors that act by different mechanisms. Kif15-IN-1 arrests the motor in a microtubule-bound state and thus blocks motility without disrupting its ability to cross-link microtubules (Milic *et al.*, 2018) (Figure 3A). In contrast, GW108X prevents the motor domain of Kif15 from binding the microtubule track, thus preventing the formation of microtubule cross-links (Dumas *et al.*, 2019) (Figure 3B). Both of these Kif15 inhibitors cause some alterations in overall spindle morphology (see *Materials and Methods*; Supplemental Figure S1E), but for these experiments we selected spindles whose form was as close to normal as possible.

Unexpectedly due to Kif15's plus-end-directed motor activity, disruption of Kif15 microtubule binding by GW108X causes significant disruption to spindle repair. Under this condition, repair is even

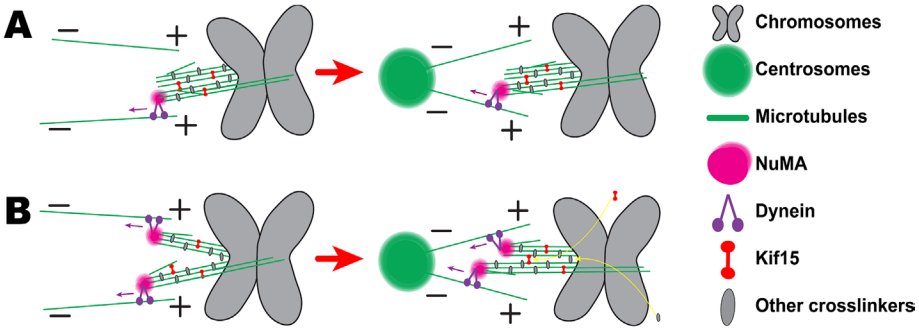

FIGURE 4: Kif15 cross-linking encourages the formation and maintenance of cohesion between k-fiber associated microtubules. (A, B) During spindle repair, the microtubules associated with some k-fiber stubs remain tightly bound together, while others splay apart. (A) Microtubule pairs cross-linked by Kif15 often withstand spindle forces during poleward transport. (B) When k-fiber stubs splay, Kif15 re-cross-links microtubules to zip up splayed k-fiber stubs. When Kif15 microtubule binding is perturbed, k-fiber stubs are more likely to splay even before, or in the absence of, poleward transport.

more delayed than in NuMA siRNA spindles (Figure 3B; Supplemental Figure S1C; Supplemental Video S3). Around 25% of the time, spindles treated with GW108X fail to repair altogether during observation, leaving the k-fiber still unattached to the pole at the end of filming, a behavior that was very rare in control spindles (occurring around 3% of the time) (Supplemental Figure S1A). While the average time until repair is normal with KIF15-IN-1 (Supplemental Figure S1C), it is slightly more common for these spindles not to undergo detectable repair during imaging than control spindles (~10% of the time; Supplemental Figure S1A). Poleward transport of severed microtubule minus-ends has been strongly coupled with minus-end-directed force production by dynein (Elting *et al.*, 2014; Sikirzhytski *et al.*, 2014; Hueschen *et al.*, 2017); thus the apparent additional requirement for Kif15, a plus-end-directed motor, in efficient poleward transport is surprising. We tested whether inhibition by GW108X affected recruitment of NuMA to ablated k-fiber minus-ends and found that it was qualitatively unaltered (Supplemental Figure S1F). Thus, we speculate that Kif15 is likely not directly involved in repair, but that Kif15-mediated cross-linking might help mechanically anchor track microtubules on which the NuMA/dynein complex walks when transporting ablated k-fiber stubs, or that effective poleward transport of ablated k-fibers requires normal k-fiber architecture, which may be disrupted when Kif15 is inhibited (see below).

Since inhibiting the ability of Kif15 to cross-link microtubules seems to slow and delay poleward transport of ablated k-fiber stubs, we expected a similar reduction of splaying, when compared with control spindles, as we saw in the NuMA depletion experiments. We indeed observed that stub splaying in cells treated with KIF15-IN-1 occurs with roughly the same frequency, duration, and magnitude as in untreated cells (Figure 3C-E; Supplemental Figure S1, A and G). In contrast, GW108X treatment exacerbates splaying. For instance, when ablated k-fiber stubs in GW108X-treated cells splay, they often remain splayed for longer, a phenomenon not observed in cells treated with KIF15-IN-1 (Figure 3C). On average, these k-fiber stubs also undergo more cumulative splaying over the course of the entire spindle repair process, demonstrating that Kif15 cross-linking is instrumental in the maintenance and reformation of intermicrotubule bonds within ablated k-fiber stubs (Figure 3D). The appearance of this effect specifically following exposure to GW108X, but not KIF15-IN-1, suggests that the function of Kif15 most relevant to k-fiber stub splaying is intermicrotubule cross-linking, not motor activity. Furthermore, the increased total splaying for GW108X-treated k-fiber stubs occurs despite decreased poleward transport, as shown by tracking the kinetochore's poleward displacement over the same period (Figure 3E). These data further point to the conclusion that the pronounced splaying results specifically from the loss of Kif15 cross-linking, independent of the effects of GW108X treatment on poleward transport.

We also qualitatively observed altered morphology even in unsevered k-fibers in GW108X-treated spindles, which, unlike untreated spindles, sometimes splay apart along their lengths (Figure 3F). While we did not typically observe GW108X-treated spindles to splay, when it occurred, it tended to be during prolonged imaging with ablation and was often accompanied by modest shortening of the spindle. We presume that the spindle shortening, which we observed occasionally under prolonged imaging in all conditions, may be a result of increased compressive force present due to the dynein-powered poleward transport response. When this occurs, k-fibers are sometimes forced to bend or buckle as the poles come closer together. Frequently, in GW108X-treated cells, this buckling induces splaying in the middle of the k-fibers, resulting in microtubule bundles that are apparently connected at both the centrosome and kinetochore, but are clearly unattached along much of their lengths (Figure 3Fii). When we see similar modest shortening in untreated spindles over the course of imaging, their k-fibers do not typically splay (Figure 3Fi). These results are consistent with Kif15's role in stabilizing kinetochore-microtubules during metaphase (Gayek and Ohi, 2014).

Altogether, these data suggest that, in addition to contributing to outward spindle-axis force generation, Kif15 promotes the mechanical cohesion of microtubules associated with k-fibers along their lengths by cross-linking microtubules to form and maintain tightly bound bundles. By doing so, Kif15 helps the k-fiber both maintain its structural integrity under duress and, when its characteristic structure has been compromised, efficiently reform into a cohesive parallel microtubule array (Figure 4). This function of Kif15 in k-fiber structural maintenance might be particularly critical in other mammalian cell types in which k-fibers face additional mechanical challenges and constraints, such as crowding from higher numbers of chromosomes. It will also be interesting to investigate whether this function is further supported by molecular redundancy from other cross-linkers that localize to k-fibers, such as the clathrin/TACC3/ch-TOG complex and HURP. These or other molecules might contribute additional support to the mechanical redundancy Kif15 brings to the k-fiber, with microtubules reinforcing each other to help ensure accurate spindle attachment and chromosome segregation. Such a balance between molecular force generators might help k-fibers reshape themselves in response to spindle dynamics.

MATERIALS AND METHODS

Request a protocol through *Bio-protocol*.

Cell culture

Wild-type Ptk2 cells and Ptk2 cells stably expressing GFP-α-tubulin (both a gift of Sophie Dumont, UCSF) were cultured in MEM (Genesee 25-504 or Fisher 11095080) supplemented with nonessential amino acids (Genesee 25-536), sodium pyruvate (Genesee 25-537),

penicillin/streptomycin (Genesee 25-512), and heat-inactivated fetal bovine serum (Genesee 25-514H). For live imaging, cells were plated in 9.6-cm^2 glass-bottom dishes treated with poly-D-lysine (MatTek P35GC-1.5-14-C) in 2 ml of MEM-complete (described above). For immunofluorescence experiments, cells were plated on #1.5 25-mm coverslips (HCl cleaned and treated with poly-L-lysine) in a 6-well plate.

Treatment with small molecule inhibitors

We found that effective dosages for small molecule inhibitors KIF15-IN-1 and GW108X varied somewhat between batches, and so we screened each new batch for the minimum effective dose where we could observe a phenotype. For treatment with KIF15-IN-1 (Apex Bio), inhibitor was added to plated cells at a final concentration 12.5–50 µM (from 5–10 mM stock in DMSO) and imaging was performed 1–3 h after treatment. For treatment with GW108X (custom synthesis as previously described [Dumas *et al.*, 2019]), inhibitor was added to plated cells at a final concentration 25-100 µM (from 10 mM stock in DMSO) and imaging was performed within 1 h of treatment. For treatment with STLC (Sigma-Aldrich 164739-5G), inhibitor was added to plated cells at a final concentration 5 µM (from 20 mM stock in DMSO) and imaging was performed within 1 h of treatment. For treatment with nocodazole (MilliporeSigma 48-792-910MG), inhibitor was added to plated cells at a final concentration 20–40 nM (from 2 mM stock in DMSO) and imaging was performed within 1 h of treatment. Using these conditions, morphological signs of inhibition were detectable in the presence of all inhibitors. In the case of KIF15-inhibition, such signs included shortened spindles (Supplemental Figure S1E). In the case of both GW108X and KIF15-IN-1, we also observed qualitative increases in the number of nonbioriented chromosomes and of k-fibers that were not fully integrated into poles. However, for these studies, we selected spindles that were as morphologically normal as possible. In the case of STLC, we observed many monopolar spindles, although we selected bipolar spindles (which had presumably formed before addition of inhibitor) for these studies. In the case of nocodazole, similar to Ki15-inhibition, we verified inhibition using morphological changes in spindle structure, particularly shortened spindles.

Transfections & siRNA

For NuMA siRNA experiments, GFP-α-tubulin expressing Ptk2 cells were transfected with siRNA for NuMA as previously described (Udy *et al.*, 2015; Elting *et al.*, 2017). The sequence for our siNuMA was 5′-GCATAAAGCGGAGACUAAA-3′, designed based on the Ptk2 transcriptome, and Oligofectamine (Invitrogen 12252-011) was used for transfection reagent (Udy *et al.*, 2015; Elting *et al.*, 2017). Transfected plates were either fixed or imaged live 48–96 h following treatment, with most experiments conducted on the third day after transfection. We verified knockdown by observing NuMA expression and localization in fixed cells via immunofluorescence assay (Figure 1A). In live cells, we also frequently observed spindle abnormalities, such as splayed or multiple poles, further verifying successful NuMA knockdown. However, we chose cells with bipolar spindles for ablation experiments in order to focus on a direct effect of NuMA rather than effects of perturbing overall spindle architecture.

For time-lapse imaging of postablation NuMA recruitment in Kif15-inhibited cells, plates were cotransfected with mCherry-tubulin (human α-tubulin in pmCherry-C1, Takara Bio; constructed by Michael Davison; gift of Sophie Dumont) and GFP-NuMA (human NuMA in pEGFP-N1, Takara Bio; constructed by Duane Compton group [Kisurina-Evgenieva *et al.*, 2004]; gift of Sophie Dumont) 48–96 h prior to imaging live using ViaFect Transfection Reagent (Promega; Elting *et al.*, 2014). Before imaging, cells were treated with either Kif15-IN-1 or GW108X as described in the section *Treatment with small molecule inhibitors*. Imaging procedures and conditions are outlined in the section *Live cell imaging and laser ablation*. Here we used 240-ms exposures for both the 488-nm (GFP) and 561-nm (mCherry) diode lasers. Ablations were performed in spindles strongly expressing GFP at their poles and whose morphology suggested successful Kif15 inhibition, as detailed in the section *Treatment with small molecule inhibitors*.

Immunofluorescence

Immunofluorescence was used to verify knockdown by siRNA of NuMA. For fixation, cells were treated for 3 min with a solution of 95% methanol and 4.8 mM EGTA. The following antibodies were used for these experiments: mouse anti-α-tubulin DM1α (1:500, Invitrogen 62204), rabbit anti-NuMA (1:400, Novus Biologicals NB500-174SS), human anti-centromere protein (CREST; 1:25, Antibodies Inc 15-234) (stained but not shown), fluorescent secondary antibodies (1:500, Invitrogen), and Hoechst 33342 (Invitrogen H3570). Coverslips were mounted on slides using Prolong Gold. Following fixation, cells were imaged using the confocal fluorescence microscope described below. For verifying knockdown, identical conditions (for fixation, staining, and imaging) were used to compare knockdown and control cells.

Live cell imaging and laser ablation

For live cell imaging, cells were plated in 9.6-cm^2 glass-bottom poly-D-lysine-coated dishes (MatTek P35GC-1.5-14-C) in 2 ml of MEM-complete (described above) and left in an incubator at 37°C and 5% CO_2 until time for imaging.

Live imaging and ablation experiments were performed essentially as previously described (Elting *et al.*, 2017). In this case, live imaging was performed on a Nikon Ti-E stand on an Andor Dragonfly spinning disk confocal fluorescence microscope; spinning disk dichroic Chroma ZT405/488/561/640rpc; 488-nm (50 mW) diode laser (240-ms exposures) with Borealis attachment (Andor); emission filter Chroma Chroma ET525/50m; and an Andor iXon3 camera. Imaging was performed with a 100× 1.45 Ph3 Nikon objective and a 1.5× magnifier (built-in to the Dragonfly system). Frames were collected every 0.3–4.0 s for up to ~4 min after ablation. Targeted laser ablation was performed using an Andor Micropoint attachment with galvo-controlled steering to deliver 20–30 3-ns pulses at 20 Hz of 551 nm light. Andor Fusion software was used to control acquisition and Andor IQ software was used to simultaneously control the laser ablation system. For all experiments involving live cells, imaging was conducted on a closed stage top incubator (Okolab), which maintains conditions of 30°C, 5% CO_2, and humidity.

Data analysis

Fiji was used to prepare all videos for analysis. This process consisted of cropping frames, adjusting brightness and contrast, and converting file types. We cropped GFP-α-tubulin ablation images in order to more clearly track the positions and splay angles of ablated k-fiber stubs. Videos were saved as both a TIFF stack and an AVI copy for each. The "No Compression" option in FIJI was used when saving videos as AVI files. Linear adjustments were made to the brightness and contrast of immunofluorescence, cotransfection, and GFP-α-tubulin ablation videos. The brightness and contrast of all videos in each immunofluorescence and cotransfection data were scaled the same as all other videos in the set.

In videos of GFP-α-tubulin spindles, spindle length was measured using the "line" tool in Fiji. These measurements were

conducted at the beginning of imaging of the spindle to prevent potential effects on spindle length of long-term imaging. Poles were identified as the center of high-intensity circles at the spindle ends. The focus of radial microtubule bundles was designated as the pole position for poles that were out of focus or dim.

Following ablations, k-fiber stubs first drifted away from the pole, toward the spindle midzone, before being transported poleward. When a k-fiber stub was not visibly transported poleward during at least 4 min of imaging, this was counted as an instance in which spindle repair (and poleward transport) did not transpire. We define poleward transport onset as the time at which the distance between the ablated k-fiber stub's kinetochore and the pole is maximal. This was done via a tracking program, written in Python, for videos in which both the kinetochore and pole remain visible throughout. Poles were identified in a manner similar to that used to measure spindle length and kinetochore positions were defined as k-fiber stub plus-ends. Video playback was used, as many times as needed, to verify all pole and kinetochore position measurements.

Another tracking program, home-written in Python, was used to measure ablated k-fiber stub splay angle. For videos in which the k-fiber stub was visible throughout, the splay angle was defined as the angle formed by the k-fiber stub's plus-end and the minus-ends of the two most separated splayed microtubule bundles. Occasionally, microtubule bundles were not approximately straight. In this case, instead of clicking on the bundle's minus-end, clicks were made somewhere along the bundle's length so that the measured splay angle more accurately reflects the angle between the bundles proximal to the kinetochore. All splay angle measurements are verified by video playback, as many times as needed. Splay durations were measured as the length of uninterrupted time for which a k-fiber stub was splayed at an angle greater than 15°. Before applying this splay angle threshold, splay angle versus time data were smoothed using a 7-point binomial filter (Marchand and Marmet, 1983; Aubury and Luk, 1996; Figure 2, A and B; Figure 3C; Supplemental Figure S1D), making it easier to identify the initiation and conclusion of each splaying event. This same filter was applied to the k-fiber stub displacement versus time data for calculating the instantaneous velocity (Figure 2, A and B).

ACKNOWLEDGMENTS

We thank Sophie Dumont, Dick McIntosh, Claire Walczak, Christina Hueschen, Jon Kuhn, Alex Long, and Elting Lab members for helpful discussions about the work. We thank Sophie Dumont (UCSF) for the gift of Ptk2 cells expressing GFP-α-tubulin and of plasmids. We thank Eva Johannes and Mariusz Zareba of the North Carolina State University Cellular and Molecular Imaging Facility for helpful discussions and assistance with microscopy. MWE, MAB, and MGS are supported by a Ralph E. Powe Junior Faculty Enhancement Award from the Oak Ridge Associated Universities and NIH R35GM138083. R.O. and A.L.S. are supported by R01GM086610.

REFERENCES

Aubury M, Luk W (1996). Binomial filters. J VLSI Signal Process Syst Signal Image Video Technol 12, 35–50.

Bird AW, Hyman Aa (2008). Building a spindle of the correct length in human cells requires the interaction between TPX2 and Aurora A. J Cell Biol 182, 289–300.

Booth DG, Hood FE, Prior IA, Royle SJ (2011). A TACC3/ch-TOG/clathrin complex stabilises kinetochore fibres by inter-microtubule bridging. EMBO J 30, 906–919.

Brouhard GJ, Rice LM (2018). Microtubule dynamics: an interplay of biochemistry and mechanics. Nat Rev Mol Cell Biol 19, 451–463.

Brugués J, Nuzzo V, Mazur E, Needleman DJ (2012). Nucleation and transport organize microtubules in metaphase spindles. Cell 149, 554–564.

Cameron LA, Yang G, Cimini D, Canman JC, Kisurina-Evgenieva O, Khodjakov A, Danuser G, Salmon ED (2006). Kinesin 5–independent poleward flux of kinetochore microtubules in PtK1 cells. J Cell Biol 173, 173–179.

Cassimeris L, Salmon ED (1991). Kinetochore microtubules shorten by loss of subunits at the kinetochores of prometaphase chromosomes. J Cell Sci 98 (Pt 2), 151–158.

Cheeseman LP, Harry EF, McAinsh AD, Prior IA, Royle SJ (2013). Specific removal of TACC3–ch-TOG–clathrin at metaphase deregulates kinetochore fiber tension. J Cell Sci 126, 2102–2113.

Dionne MA, Howard L, Compton DA (1999). NuMA is a component of an insoluble matrix at mitotic spindle poles. Cell Motil Cytoskeleton 42, 189–203.

Drechsler H, McHugh T, Singleton MR, Carter NJ, McAinsh AD (2014). The Kinesin-12 Kif15 is a processive track-switching tetramer. Elife 3, e01724.

Drummond DR (2011). Regulation of microtubule dynamics by kinesins. Semin Cell Dev Biol 22, 927–934.

Dumas ME, Geng-Yuan C, Kendrick ND, Xu G, Larsen SA, Jana S, Waterson AG, Bauer JA, Hancock W, Sulikowski GA, *et al.* (2019). Dual inhibition of Kif15 by oxindole and quinazolinedione chemical probes. Bioorganic & Medicinal Chemistry Letters 29, 148–154.

Elting MW, Hueschen CL, Udy DB, Dumont S (2014). Force on spindle microtubule minus ends moves chromosomes. J Cell Biol 206, 245–256.

Elting MW, Prakash M, Udy DB, Dumont S (2017). Mapping load-bearing in the mammalian spindle reveals local kinetochore fiber anchorage that provides mechanical isolation and redundancy. Curr Biol 27, 2112–2122.e5.

Elting MW, Suresh P, Dumont S (2018). The Spindle: Integrating architecture and mechanics across scales. Trends Cell Biol 28, 896–910.

Gaglio T, Dionne MA, Compton DA (1997). Mitotic spindle poles are organized by structural and motor proteins in addition to centrosomes. J Cell Biol 138, 1055–1066.

Gaglio T, Saredi A, Bingham JB, Hasbani MJ, Gill SR, Schroer TA, Compton DA (1996). Opposing motor activities are required for the organization of the mammalian mitotic spindle pole. J Cell Biol 135, 399–414.

Gayek AS, Ohi R (2014). Kinetochore-microtubule stability governs the metaphase requirement for Eg5. Mol Biol Cell 25, 2051–2060.

Goshima G, Nédélec F, Vale RD (2005). Mechanisms for focusing mitotic spindle poles by minus end-directed motor proteins. J Cell Biol 171, 229–240.

Hays TS, Salmon ED (1990). Poleward force at the kinetochore in metaphase depends on the number of kinetochore microtubules. J Cell Biol 110, 391–404.

Hays TS, Wise D, Salmon ED (1982). Traction force on a kinetochore at metaphase acts as a linear function of kinetochore fiber length. J Cell Biol 93, 374–389.

Hueschen CL, Kenny SJ, Xu K, Dumont S (2017). NuMA recruits dynein activity to microtubule minus-ends at mitosis. Elife 6, e29328.

Kajtez J, Solomatina A, Novak M, Polak B, Vukušić K, Rüdiger J, Cojoc G, Milas A, Šestak IŠ, Risteski P, *et al.* (2016). Overlap microtubules link sister k-fibres and balance the forces on bi-oriented kinetochores. Nat Commun 7, 10298.

Kapitein LC, Peterman EJG, Kwok BH, Kim JH, Kapoor TM, Schmidt CF (2005). The bipolar mitotic kinesin Eg5 moves on both microtubules that it crosslinks. Nature 435, 114–118.

Kapoor TM, Mayer TU, Coughlin ML, Mitchison TJ (2000). Probing spindle assembly mechanisms with monastrol, a small molecule inhibitor of the mitotic kinesin, Eg5. J Cell Biol 150, 975–988.

Kisurina-Evgenieva O, Mack G, Du Q, Macara I, Khodjakov A, Compton DA (2004). Multiple mechanisms regulate NuMA dynamics at spindle poles. J Cell Sci 117, 6391–6400.

Lampson MA, Renduchitala K, Khodjakov A, Kapoor TM (2004). Correcting improper chromosome-spindle attachments during cell division. Nat Cell Biol 6, 232–237.

Long AF, Suresh P, Dumont S (2020). Individual kinetochore-fibers locally dissipate force to maintain robust mammalian spindle structure. J Cell Biol 219, e201911090.

Ma HT, Erdal S, Huang S, Poon RYC (2014). Synergism between inhibitors of Aurora A and KIF11 overcomes KIF15-dependent drug resistance. Mol Oncol 8, 1404–1418.

Maiato H, Rieder CL, Khodjakov A (2004). Kinetochore-driven formation of kinetochore fibers contributes to spindle assembly during animal mitosis. J Cell Biol 167, 831–840.

Malaby HLH, Dumas ME, Ohi R, Stumpff J (2019). Kinesin-binding protein ensures accurate chromosome segregation by buffering KIF18A and KIF15. J Cell Biol 218, 1218–1234.

Mann BJ, Balchand SK, Wadsworth P (2017). Regulation of Kif15 localization and motility by the C-terminus of TPX2 and microtubule dynamics. Mol Biol Cell 28, 65–75.
Marchand P, Marmet L (1983). Binomial smoothing filter: A way to avoid some pitfalls of least-squares polynomial smoothing. Rev Sci Instrum 54, 1034–1041.
Mayr MI, Hümmer S, Bormann J, Grüner T, Adio S, Woehlke G, Mayer TU (2007). The human kinesin Kif18A is a motile microtubule depolymerase essential for chromosome congression. Curr Biol 17, 488–498.
McDonald KL, O'Toole ET, Mastronarde DN, McIntosh JR (1992). Kinetochore microtubules in PTK cells. J Cell Biol 118, 369–383.
McHugh T, Drechsler H, McAinsh AD, Carter NJ, Cross RA (2018). Kif15 functions as an active mechanical ratchet. Mol Biol Cell 29, 1743–1752.
Merdes A, Ramyar K, Vechio JD, Cleveland DW (1996). A complex of NuMA and cytoplasmic dynein is essential for mitotic spindle assembly. Cell 87, 447–458.
Milic B, Chakraborty A, Han K, Bassik MC, Block SM (2018). KIF15 nanomechanics and kinesin inhibitors, with implications for cancer chemotherapeutics. Proc Natl Acad Sci USA 115, E4613–E4622.
Mitchison TJ (1989). Polewards microtubule flux in the mitotic spindle: evidence from photoactivation of fluorescence. J Cell Biol 109, 637–652.
Nicklas RB, Kubai DF, Hays TS (1982). Spindle microtubules and their mechanical associations after micromanipulation in anaphase. J Cell Biol 95, 91–104.
Nixon FM, Gutiérrez-Caballero C, Hood FE, Booth DG, Prior IA, Royle SJ (2015). The mesh is a network of microtubule connectors that stabilizes individual kinetochore fibers of the mitotic spindle. Elife 4, 1–21.
Pereira AJ, Maiato H (2012). Maturation of the kinetochore-microtubule interface and the meaning of metaphase. Chromosome Res 20, 563–577.
Qiao Y, Chen J, Ma C, Liu Y, Li P, Wang Y, Hou L, Liu Z (2018). Increased KIF15 expression predicts a poor prognosis in patients with lung adenocarcinoma. Cell Physiol Biochem 51, 1–10.
Raaijmakers JA, van Heesbeen R, Meaders JL, Geers EF, Fernandez-Garcia B, Medema RH, Tanenbaum ME (2012). Nuclear envelope-associated dynein drives prophase centrosome separation and enables Eg5-independent bipolar spindle formation. EMBO J 31, 4179–4190.
Rath O, Kozielski F (2012). Kinesins and cancer. Nat Rev Cancer 12, 527–539.
Reinemann DN, Sturgill EG, Das DK, Degen MS, Vörös Z, Hwang W, Ohi R, Lang MJ (2017). Collective force regulation in anti-parallel microtubule gliding by dimeric Kif15 kinesin motors. Curr Biol 27, 2810–2820.e6.
Rieder CL (1981). The structure of the cold-stable kinetochore fiber in metaphase PtK1 cells. Chromosoma 84, 145–158.
Royle SJ, Bright NA, Lagnado L (2005). Clathrin is required for the function of the mitotic spindle. Nature 434, 1152–1157.
Saxton WM, Stemple DL, Leslie RJ, Salmon ED, Zavortink M, McIntosh JR (1984). Tubulin dynamics in cultured mammalian cells. J Cell Biol 99, 2175–2186.
Sheykhani R, Baker N, Gomez-Godinez V, Liaw L-H, Shah J, Berns MW, Forer A (2013). The role of actin and myosin in PtK2 spindle length changes induced by laser microbeam irradiations across the spindle. Cytoskeleton 70, 241–259.
Sikirzhytski V, Magidson V, Steinman JB, He J, Berre ML, Tikhonenko I, Ault JG, McEwen BF, Chen JK, Sui H, *et al*. (2014). Direct kinetochore-spindle pole connections are not required for chromosome segregation. J Cell Biol 206, 231–243.
Silljé HHW, Nagel S, Körner R, Nigg EA (2006). HURP is a Ran-Importin β-regulated protein that stabilizes kinetochore microtubules in the vicinity of chromosomes. Curr Biol 16, 731–742.
Spurck TP, Stonington OG, Snyder JA, Pickett-Heaps JD, Bajer A, Mole-Bajer J (1990). UV microbeam irradiations of the mitotic spindle. II. Spindle fiber dynamics and force production. J Cell Biol 111, 1505–1518.
Sturgill EG, Das DK, Takizawa Y, Shin Y, Collier SE, Ohi MD, Hwang W, Lang MJ, Ohi R (2014). Kinesin-12 Kif15 targets kinetochore fibers through an intrinsic two-step mechanism. Curr Biol 24, 2307–2313.
Sturgill EG, Ohi R (2013). Kinesin-12 differentially affects spindle assembly depending on its microtubule substrate. Curr Biol 23, 1280–1290.
Sun Y-F, Wu H-L, Shi R-F, Chen L, Meng C (2020). KIF15 promotes proliferation and growth of hepatocellular carcinoma. Anal Cell Pathol 2020, 6403012.
Suresh P, Long AF, Dumont S (2020). Microneedle manipulation of the mammalian spindle reveals specialized, short-lived reinforcement near chromosomes. Elife 9, e53807.
Tanenbaum ME, Macůrek L, Janssen A, Geers EF, Alvarez-Fernández M, Medema RH (2009). Kif15 cooperates with eg5 to promote bipolar spindle assembly. Curr Biol 19, 1703–1711.
Terribas E, Fernández M, Mazuelas H, Fernández-Rodríguez J, Biayna J, Blanco I, Bernal G, Ramos-Oliver I, Thomas C, Guha R, *et al*. (2020). KIF11 and KIF15 mitotic kinesins are potential therapeutic vulnerabilities for malignant peripheral nerve sheath tumors. Neuro Oncol Adv 2, i62–i74.
Tsuchiya K, Hayashi H, Nishina M, Okumura M (2018). Importin-β targets HURP to kinetochore-fibers in coordination with Ran-GTP in human mitotic cells. bioRxiv.
Udy DB, Voorhies M, Chan PP, Lowe TM, Dumont S (2015). Draft de novo transcriptome of the rat kangaroo Potorous tridactylus as a tool for cell biology. PLoS One 10, e0134738.
Vladimirou E, Mchedlishvili N, Gasic I, Armond JW, Samora CP, Meraldi P, McAinsh AD (2013). Nonautonomous movement of chromosomes in mitosis. Dev Cell 27, 60–71.
Walczak CE (2000). Microtubule dynamics and tubulin interacting proteins. Curr Opin Cell Biol 12, 52–56.
Wang J, Guo X, Xie C, Jiang J (2017). KIF15 promotes pancreatic cancer proliferation via the MEK–ERK signalling pathway. Br J Cancer 117, 245–255.
Ye F, Tan L, Yang Q, Xia Y, Deng L-W, Murata-Hori M, Liou Y-C (2011). HURP regulates chromosome congression by modulating kinesin Kif18A function. Curr Biol 21, 1584–1591.
Yu X, He X, Heindl LM, Song X, Fan J, Jia R (2019). KIF15 plays a role in promoting the tumorigenicity of melanoma. Exp Eye Res 185, 107598.
Zhai Y, Kronebusch PJ, Borisy GG (1995). Kinetochore microtubule dynamics and the metaphase-anaphase transition. J Cell Biol 131, 721–734.
Zhao H, Bo Q, Wu Z, Liu Q, Li Y, Zhang N, Guo H, Shi B (2019). KIF15 promotes bladder cancer proliferation via the MEK-ERK signaling pathway. Cancer Manag Res 11, 1857–1868.